SLAC–PUB–6400
December 1993
(E)

QUANTUM-MECHANICAL SUPPRESSION OF BREMSSTRAHLUNG*

THE SLAC E146 COLLABORATION:

Ralph Becker-Szendy[1], Perry Anthony[1,2], Peter Bosted[3], Matteo Cavalli-Sforza[4], Lew Keller[1], Linda Kelley[4], Spencer Klein[4], Gary Niemi[1], Martin Perl[1], Leon Rochester[1], Joe White[3]

[1] *Stanford Linear Accelerator Center, Stanford University, Stanford, CA 94309, USA*
[2] *Laurence Livermore National Laboratory, Livermore, CA 94551, USA*
[3] *The American University, Washington, DC 20016, USA*
[4] *Santa Cruz Institute for Particle Physics, University of California, Santa Cruz, CA 95064, USA*

ABSTRACT

We have studied quantum-mechanical suppression of bremsstrahlung of low-energy 1–500 MeV photons from high-energy 25 GeV electrons. We measured the LPM effect, where multiple scattering of the radiating electron destroys coherence required for the emission of low-energy photons, and the dielectric effect, where the emitted photon traveling in the radiator medium interferes with itself. For the experiment, the collaboration developed a novel method of extracting a parasitic low-intensity high-energy electron beam into the fixed target area during normal SLC operation of the accelerator. The results agree quantitatively with Migdal's calculation of the LPM effect. Surface effects, for which there is no satisfactory theoretical prediction, are visible at low photon energies. For very thin targets, the suppression disappears, as expected. Preliminary results on dielectric suppression of bremsstrahlung are in qualitative agreement with the expectation.

1. Theoretical Expectation

Bremsstrahlung has been well understood since Bethe and Heitler's work in 1935.[1] The process is shown in Fig. 1(a). An electron of momentum p_e (with $\gamma = E_e/m_e$) traverses a radiator characterized by atomic number Z, density ρ, and radiation length X_0 and emits a photon of energy E and momentum k. To balance energy and momentum, a virtual photon q has to be exchanged with a nucleus from the radiator. The main results of Bethe and Heitler which are relevant here are: the spectrum of emitted photons is $dN_\gamma/dE \propto 1/E$, and the typical emission angle is $\theta = 1/\gamma$.

A semi-classical argument[2] for quantum-mechanical suppression of bremsstrahlung can be made by considering the longitudinal momentum $q_\parallel$ of the virtual photon:

$$q_\parallel = p_e - p'_e - k \approx \frac{m_e^2 E}{2E_e(E_e - k)} \approx \frac{E}{2\gamma^2}. \qquad (1)$$

For example, for a 100 MeV photon emitted from a 25 GeV electron, $q_\parallel$ is $0.02\,\mathrm{eV}/c$. The uncertainty relation requires that any process with such a small momentum

*Work supported by Department of Energy contracts DE–AC03–76SF00515 (SLAC) and W–4705–ENG–48 (LLNL), and National Science Foundation grants NSF–PHY–9113428 (UCSC) and NSF–PHY–9114958 (American University).

Presented at the 21st Annual SLAC Summer Institute on Particle Physics; Spin Structure in High-Energy Processes, Stanford, CA, July 26–August 6, 1993; and the 23rd International Symposium on Ultra-High-Energy Multiparticle Phenomena, Aspen, CO, September 12–17, 1993.

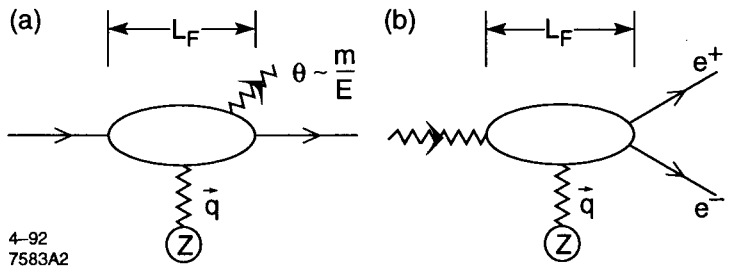

Figure 1: Feynman diagram for bremsstrahlung (a) and pair creation (b).

transfer take place over an extended distance, which we call the formation zone, with length

$$L_F = h/q_{\|} = 2\gamma^2 ch/E, \tag{2}$$

or smaller if it is limited by other effects at low photon energies. For the above numeric example, the length of the formation zone is 60 μm. In the semi-classical picture, the emission of the bremsstrahlung photon and the exchange of the virtual photon take place over the whole formation zone, but only if both the electron and the emitted photon remain undisturbed and coherent over L_F. Quantum-mechanical suppression of bremsstrahlung occurs if the coherence of either is destroyed.

1.1. LPM Effect

The most common example of an interaction which can destroy this coherence is multiple scattering. In the semi-classical picture, bremsstrahlung is suppressed if the electron multiple-scatters by an angle larger than the photon emission angle θ. The typical multiple-scattering angle is $\theta_{MS}^2 \approx (21\,\mathrm{MeV}/E_e)^2\,(L_F/X_0)$. Comparing this to Eq. 2 shows that bremsstrahlung is suppressed for $E < E_e^2/E_{LPM}$, where $E_{LPM} = m_e^2 X_0 \alpha/4\pi\hbar c$ is a material-dependent constant.

For example, for 25 GeV electrons in a uranium target, suppression occurs for $E < 265\,\mathrm{MeV}$. This effect was first suggested by Landau and Pomeranchuk in 1953,[3] and the full quantum-mechanical scattering theory was worked out by Migdal in 1956.[4] In the energy region in which this suppression occurs, the photon spectrum is modified to $dN/dE \propto 1/\sqrt{E}$.

1.2. Dielectric Suppression

Even though the LPM effect modifies the emitted photon spectrum at low energies to be proportional to $1/\sqrt{E}$, the bremsstrahlung process is still infrared-divergent, with an infinite number of photons of very low energy. Another mechanism cures that: dielectric suppression,[5] also known as the longitudinal density effect.

In the above semi-classical picture, the bremsstrahlung photon which is being emitted also needs to be coherent. It is, however, moving in a medium with a non-unity index of refraction, and the contributions to it will be phase shifted along

the length L_F. The criterion that the photon not interfere destructively with itself yields suppression for $E < \gamma\omega_P$, where ω_P is the plasma frequency of the radiator, not very material dependent. For example, in the case of 25 GeV electrons this suppression occurs for photon energies below 3.5 MeV in carbon targets. Below that energy, the spectrum is modified to $dN/dE \propto E$, which cures the infrared divergence.

1.3. Thin Targets

For thin targets, the above reasoning needs to be modified. For a target much thinner than L_F, the above argument shows that there is neither enough multiple scattering nor photon phase shift to disrupt bremsstrahlung, therefore the Bethe-Heitler spectrum should hold. Since $L_F \propto 1/E$ at the photon energies considered here, any target eventually becomes thin on the scale of L_F.

Targets of intermediate thickness can be treated as bulk material in the center plus two surfaces of thickness $\mathcal{O}(L_F)$. The difficulty lies in how to account for surface effects. The first and last L_F of the target should not show the full effects of LPM and dielectric suppression, using the same argument as for the thin target case. Therefore surface effects will modify the expected spectrum at low photon energies. Unfortunately, there is no satisfactory theoretical treatment of the surface effects; the only available calculation[6] yields unphysical results.

1.4. Expected Spectrum

In order to make it easier to histogram the bremsstrahlung photon spectrum, which is mostly steeply falling, we plot $dN/d\log E$, since it is constant if $dN/dE \propto 1/E$. Figure 2 shows a sketch of the overall expected spectrum based on the above semi-classical arguments for a heavy target material. At high energies, Bethe-Heitler holds, and $dN/dE \propto 1/E$. Below a threshold, LPM suppression sets in, modifying the spectrum to $\propto 1/\sqrt{E}$. Below a second (lower) threshold, dielectric suppression modifies the spectrum to $\propto E$. Note that for low-Z targets, the threshold for the dielectric effect can be higher than the threshold for the LPM effect, in which case no LPM suppression occurs. The total number of photons emitted is finite. At the upper end of the photon spectrum, as the photon energy approaches the energy of the incoming electron, the spectrum falls off again, as predicted by Bethe-Heitler.

1.5. Monte-Carlo Prediction

A Monte-Carlo calculation of the expected bremsstrahlung spectrum is required to compare to the data. Migdal's formulae for the LPM effect[4] are recursive, and do not yield results in closed form. We instead use the formalism developed by Stanev and collaborators,[7] but with the table of numeric values from Migdal's paper.[4] The dielectric effect is simulated with a multiplicative factor.[8] Both LPM and dielectric suppression can be turned off, which allows calculating an unmodified Bethe-Heitler spectrum.

The Monte-Carlo correctly simulates the case in which a single electron emits more than one bremsstrahlung photon, and allows for pair-conversion and Compton

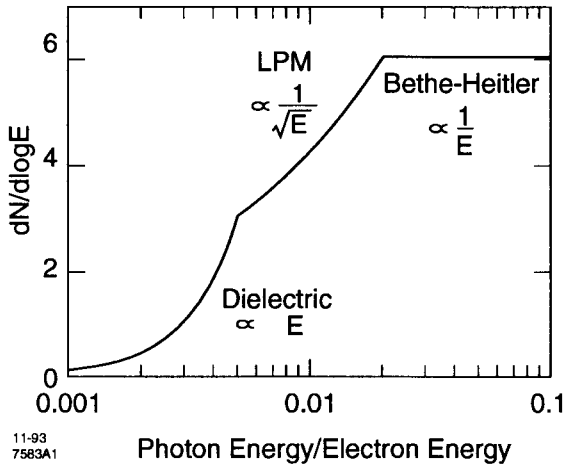

Figure 2: Sketch of the expected bremsstrahlung spectrum, with LPM and Dielectric suppression.

scattering of the produced photons. It also contains a simple but adequate model of calorimeter resolution.

2. Rationale for the Experiment

Perhaps the most important justification for doing an experiment to study these phenomena is that it is a macroscopic application of quantum mechanics in a regime not previously studied. It is rare that one can experimentally observe fundamental properties of quantum mechanics in a direct fashion.

2.1. Previous Experiments

Cosmic-ray experiments have attempted to verify the LPM and dielectric suppression; they all suffer from a lack of statistics.[9] An experiment at Serpukhov in 1975 attempted to measure LPM suppression and found qualitative agreement.[10] Unfortunately, that experiment suffered from several technical problems, and the results are not convincing. An Armenian group studied dielectric suppression as the by-product of a series of experiments which measured transition radiation;[11] the results are at best qualitative.

2.2. Related Effects

Magnetic supression is another effect which can modify the bremsstrahlung spectrum: if the electron is bent in a magnetic field by an angle larger than θ over a length L_F, bremsstrahlung is again suppressed. We have not studied this in the current experiment, since very high magnetic fields are required. An application of magnetic suppression is in high-energy e^+e^- colliders, where it suppresses beam-beam bremsstrahlung.[12]

LPM suppression also occurs in pair creation, where a photon converts to an e^+e^- pair in the Coulomb-field of a nucleus; the process is shown in Fig. 1 (b). Due to the different kinematics, however, the effect is only visible at very high energies.

There are a number of effects analogous to LPM suppression in QCD and nuclear physics. The best-known example is color transparency, where gluon bremsstrahlung from quarks traversing a nucleus is suppressed.[13]

2.3. Applications

As shown above, LPM suppression of low-energy photon bremsstrahlung is already large enough for 25 GeV electrons to be easily observable. For electrons with energies $\mathcal{O}(1\,\mathrm{TeV})$, a significant fraction of bremsstrahlung is suppressed in heavy media. Therefore electromagnetic showers from such electrons are longer and more grainy than would be expected if one ignored the LPM effect. Such high-energy electrons will be commonly observed with shower calorimeters in the next generation of accelerators such as the SSC, LHC, and e^+e^- colliders.

In natural particle physics, it is expected that the DUMAND experiment will observe deep-inelastic neutrino interactions on the Glashow resonance at 6.4 PeV: $\nu_e + \mathcal{N} \to W^- + \mathcal{N}' \to e^- + \mathcal{N}'$. Neutrinos of this energy are expected to be produced by active galactic nuclei.[14] The characteristics of an electro-magnetic shower of several PeV in water are greatly changed by the LPM effect.[15]

The LPM suppression of pair-creation is significant for EeV cosmic-ray air-shower studies and gamma-ray astronomy, in which photons of energies $\geq 10^{19}$ eV interact through pair-creation, and the resulting electro-magnetic shower is observed on the ground. The LPM effect increases the graininess of the shower, and modifies the relationship between particle density distribution measured on the ground and the energy of the primary particle.[16]

3. Experiment and Analysis

3.1. Setup

The experimental setup was quite simple and is shown schematically in Fig. 3. The beam entered End Station A and traversed thin target foils mounted in a movable target holder.[17] The targets are listed in Table 1. The materials were chosen to span a wide range in Z and X_0, so as to have targets which display varying amounts of LPM suppression in the energy region under study. The target thickness was chosen to minimize both surface effects (for thin targets) and multi-photon pileup (for thick targets). For most materials, two target thicknesses were used, which allowed us to study thickness-dependent effects. One position in the target holder contained no target, and was used to measure backgrounds.

After the target, the electrons were deflected by a magnet with $B \cdot dL = 3.25\,\mathrm{T} \cdot \mathrm{m}$ into a wire chamber used to measure the electron momentum. The 2 mm wire spacing of the chambers provides a 100 MeV momentum resolution, good enough to suppress backgrounds. Three lead-glass counters behind the wire chamber allow determination of the number of electrons in each beam spill.

Bremsstrahlung photons produced in the target continued downstream to the BGO calorimeter. The calorimeter was built in 1984 and consists of 45 BGO crystals,

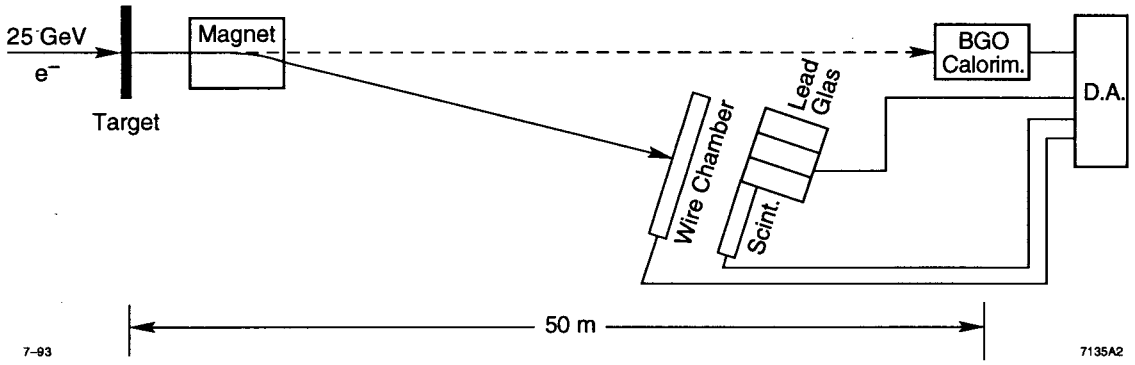

Figure 3: The layout of SLAC E146. Electrons entering End Station A traverse a thin target and are bent downward by a spectrometer magnet into a set of wire chambers and a lead glass block array. Bremsstrahlung photons emitted in the target continue downstream into a BGO calorimeter.

Table 1: Targets used in experiment E146. The last column is the semi-classical threshold energy for the LPM effect, E_e^2/E_{LPM}.

Target Material	Z	X_0 (cm)	Thickness (% X_0)	LPM Threshold (MeV)
Carbon	6	18.8	2%, 6%	4.4
Aluminum	13	8.9	3%, 6%	9.2
Iron	26	1.76	3%, 6%	47
Tungsten	74	0.35	2%, 6%	235
Gold	79	0.34	0.1%, 1%, 6%	240
Lead	82	0.56	2%	147
Uranium	92	0.32	3%, 5%	265

each measuring $2 \times 2 \times 20\,\mathrm{cm}^3$, instrumented with photomultipliers.[18] Calorimeter information was digitized by a 12-bit LeCroy 2280 ADC. Data was read out for each accelerator pulse, so there is no trigger bias. The electron and photon flight-paths visible to the calorimeter were kept in vacuum to minimize backgrounds and prevent bremsstrahlung photons from converting.

3.2. Beam

High electron energies are required to observe the LPM effect at reasonable photon energies. The cross section for bremsstrahlung is very large, so a beam of very low intensity is required. It is difficult and inefficient to operate the linear accelerator at beam intensities of typically 10^{10} e^-/pulse and obtain intensities of about one e^-/pulse with good momentum resolution. The collaboration employed a technique not previously used at SLAC[19] for obtaining a secondary beam;[20] it is illustrated in Fig. 4. During normal SLC operation, about 10% of the 50 GeV beam is removed by collimating scrapers at the end of the linac in sectors 28–30; this creates a

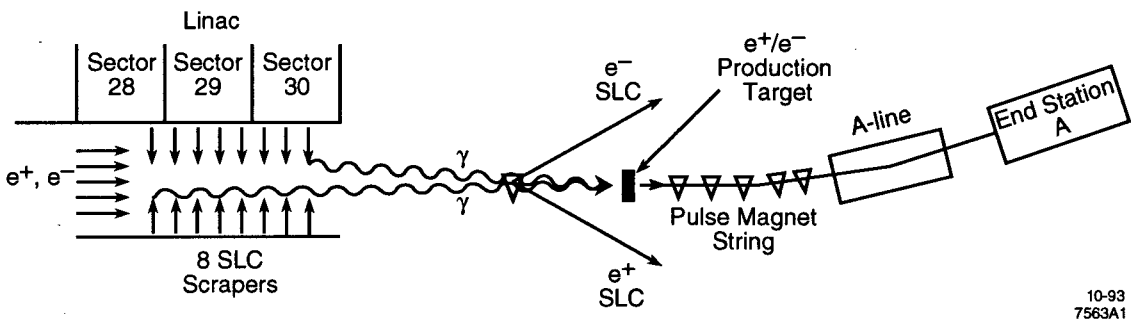

Figure 4: A diagram of the parasitic beam generation. High energy photons produced in the collimators of sectors 28–30 travel downstream, past the bending magnet that directs electrons and positrons into the SLC arcs, and onto an e^+e^- production target in the beam switchyard. Electrons produced in the target are captured by the A-line and transported to End Station A.

flux of high-energy photons traveling down the linac. After the high-energy electrons and positrons have been magnetically steered to the SLC arcs for delivery to the SLD experiment, these photons continue into the beam switchyard. A $0.7\,X_0$ copper production target was inserted into the dump line to convert some of the photons into electrons. The End Station A extraction line (consisting of a set of pulsed extraction magnets and the bending arc) then selected electrons of a specific energy, collimated them, and delivered them to the experimental area.

The performance of the parasitic beam was very good. The beam was easy to set up and straightforward to optimize, adjust, and steer. We took data at 25 and 8 GeV, at intensities averaging one e^-/pulse, at 120 pulses per second. This intensity was achieved with the momentum-defining slits in the A-line at $\Delta p/p \leq 0.1\%$. With bremsstrahlung from the very thin gold target, we increased the flux to an average of 10 e^-/pulse. For calibration, we ran the beam line at energies of 400 and 500 MeV, albeit with much reduced flux and larger spot size.

3.3. Calibration

The only part of the experiment which requires significant effort to calibrate is the BGO calorimeter. For studying the LPM effect, its gain was set such that the usable energy range is ≈5–500 MeV; for the study of dielectric suppression, the high-voltage was increased so that the usable range was ≈0.5–50 MeV. The calorimeter had been extensively studied previously,[18] at energies ranging from 40 MeV to 8 GeV. It's non-linearity is estimated to be $\leq 2\%$.

In order to calibrate the BGO calorimeter during running, we continuously acquired cosmic-ray events traversing the calorimeter close to vertically, at a rate of about 0.1 Hz. Those are used to correct the relative gain of the channels in the calorimeter.

We used dedicated runs at 400 MeV and 500 MeV to calibrate the absolute energy scale, by directing the low-energy beam directly at the BGO calorimeter. Figure 5 shows the pulse-height spectrum obtained at 500 MeV beam energy. The FWHM of the peak is 6%, compatible with resolution measurements made on this

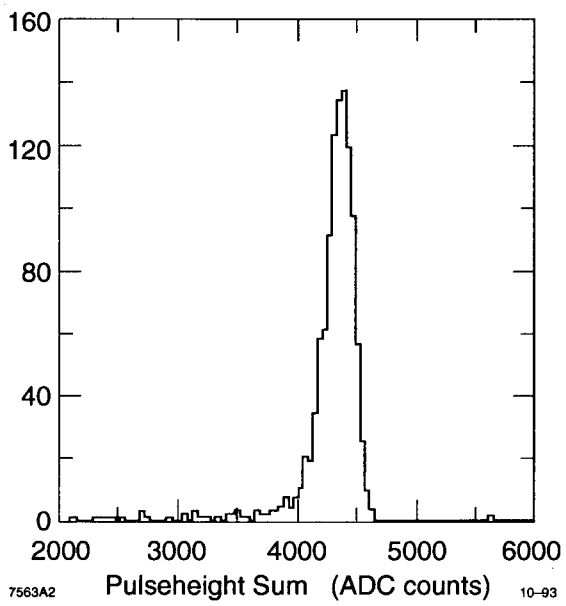

Figure 5: BGO pulseheight spectrum using a 500 MeV electron beam directly on the calorimeter.

calorimeter in 1984.[18] To calibrate the absolute energy scale for the dielectric-effect running, we currently use cosmic-ray events.

The light output of BGO is known to vary with temperature; during the experiment, the temperature of the calorimeter was monitored and recorded. This information is, however, not used in this analysis. We therefore estimate that the calibration (both absolute and relative) of the calorimeter is accurate to 10%; we expect to improve this by at least a factor of two in the final analysis.

3.4. Backgrounds

There are two fundamentally different types of backgrounds to consider. The first one is multi-photon pileup, in which a single electron traverses the target and creates more than one bremsstrahlung photon. With the angular resolution of the calorimeter, all the photons get lumped into one cluster of energy deposition. This effect is correctly handled in the Monte-Carlo program, and we consider it to be simply a part of the expected spectrum, not background.

Then there are real backgrounds. Those which are not associated with the target are synchrotron radiation from the A-line and from the electron spectrometer magnet, and mis-steered particles hitting the target holder or the beam pipe. These were studied by measuring the bremsstrahlung spectrum with no target every few hours, and found to be small enough to neglect. Typically we find less than one background photon in the calorimeter per 1000 e^-, compared to several hundred observed bremsstrahlung photons per 1000 e^-. Therefore these backgrounds are irrelevant for the study of the LPM effect. The reason that synchrotron radiation is small is that the spectrometer magnet had a very significant fringe field, which initially

bends the electrons slowly; by the time the magnetic field reaches full strength, the electron beam does not point at the calorimeter any longer. The critical energy for photons hitting the calorimeter is $\leq 100\,\mathrm{keV}$. However, these backgrounds are significant for the study of dielectric suppression and have to be reduced further; this will be discussed in Sec. 4.3.

Target-related backgrounds include transition radiation and photonuclear interactions of the electron. Transition radiation creates on average 14 keV of photon energy per electron, with the energy limited to $\leq \gamma\omega_P$, so it is again irrelevant for the study of the LPM effect. The photonuclear cross section is much smaller than the bremsstrahlung cross section, so it does not contribute significantly either. Furthermore, most of these backgrounds create photons with an angular distribution much wider than bremsstrahlung. The absence of tails on the observed angular distribution indicates that backgrounds are insignificant.

3.5. Analysis

The analysis of the data is comparatively simple. Good events are selected; they are defined as beam spills containing exactly one electron, as observed in the lead-glass blocks, and no additional low-momentum tracks. Events with multiple electrons will be used in the final analysis to enhance the statistics; they are currently neglected. The energy deposited in the BGO calorimeter is calculated with a cluster-finding algorithm; this reduces contributions from electronic noise. As mentioned above, the energy scale is known to better than 10%; the energy resolution of the calorimeter varies from about 8% at 50 MeV to 6% at 500 MeV.

The photon energies are then histogrammed logarithmically as $dN/d\log E$, with 25 bins per decade. The histogram is normalized to 1000 single e^- events, which makes the resulting histogram have entries of a convenient single-digit magnitude. The observed spectrum is compared to the two Monte-Carlo spectra for the same target. In the current preliminary analysis, the data is normalized so it matches the Monte-Carlo spectrum at the highest energies under study, at which we expect no LPM suppression. We find that this re-normalization always agrees with the experiment to better than 7%.

In order to determine the expected flux of bremsstrahlung photons, the densities and thicknesses of the targets have to be accurately known. This is not as simple as it might appear. The density of graphite varies considerably; we determined both the geometric dimensions and the weight, and calculated the density from those measurements. Metallic uranium is soft and malleable, and the targets are thin; this precludes an accurate mechanical measurement of their thickness. We instead measured the area and weight of the uranium targets, and determined the thickness from the accurately known density. We estimate that the uncertainty of target thicknesses contributes 2% to the systematic error on the absolute bremsstrahlung cross section.

Other effects which contribute to this systematic error include the absolute normalization of the number of good single-electron events (3%), and the above-mentioned uncertainty of the absolute energy scale, which translates into a 2.5% systematic error on the flux, depending on the slope of the bremsstrahlung spectrum. We believe that Monte-Carlo approximations represent Migdal's formulae[4] to within 3%.

For the current analysis, only a part of the data taken at a beam energy of 25 GeV has been analyzed. We have further data at 8 GeV, which will enhance the analysis of dielectric suppression, because synchrotron radiation backgrounds fall off much faster than the dielectric effect.

At this preliminary stage in the analysis, we have only studied the carbon and uranium targets for the LPM effect, the three gold targets for bremsstrahlung from thin targets, and one carbon target for dielectric suppression. The data for the other targets and beam energies is currently being analyzed.

4. Results

In the following sections, the observed bremsstrahlung photon spectrum is compared to Monte-Carlo predictions. In the figures, the data is shown by the crosses, with the height indicating the statistical error per bin. The top dotted line is the Bethe-Heitler Monte-Carlo prediction which ignores both LPM and dielectric suppression, and the bottom dashed line is the Monte-Carlo prediction including both LPM and dielectric suppression.

4.1. LPM effect

Figure 6 shows the observed spectra for the two carbon targets; part (a) is for a target which is 4.1 mm $\simeq 2\%X_0$ thick and part (b) for a target which is 12.7 mm $\simeq 6\%X_0$ thick. The first thing one observes is that the predicted spectrum is not flat, even if one ignores the two quantum-mechanical suppression effects. This is due to multi-photon pileup. The solid line at the top of Fig. 6(a) shows the Bethe-Heitler spectrum ignoring multi-photon pileup. Clearly, the data exhibits the small suppression at energies below 20 MeV, which is predicted by Migdal's calculation of the LPM effect.

Figure 7 shows the corresponding spectra for the two uranium targets, part (a) for a 79 μm $\simeq 3\%X_0$ target and part (b) for a 147 μm $\simeq 5\%X_0$ target. Since LPM suppression turns on at the highest energies shown in the figure (the semi-classical threshold is 265 MeV), the two expected spectra are very dissimilar. For energies above $\approx$20 MeV, the data follows the spectrum predicted by the LPM effect, and rules out the Bethe-Heitler spectrum. Below that energy, the data diverges from the expected spectrum. This is likely to be due to surface effects discussed above: at lower and lower photon energies, as the formation zone approaches the thickness of the target, LPM suppression no longer occurs fully.

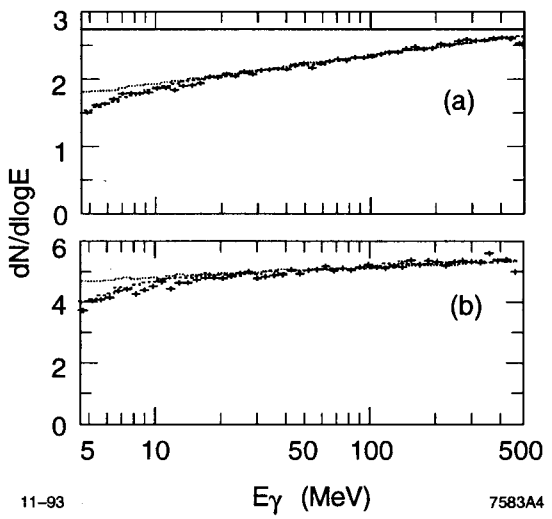

Figure 6: The observed bremsstrahlung spectrum $dN/d\log E$ (crosses) for two carbon targets, in units of photons per bin per 1000 electrons, for a 2% X_0 (a) and 6% X_0 (b) thick target. The dotted line (top) shows the Bethe-Heitler Monte-Carlo expectation, whereas the dashed line (bottom) is the Monte-Carlo expectations including the LPM effect. The solid line (top) in (a) is the Bethe-Heitler prediction ignoring multi-photon pileup.

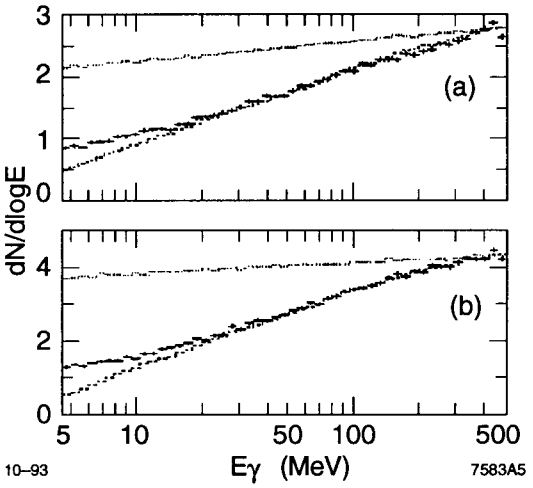

Figure 7: The observed bremsstrahlung spectrum $dN/d\log E$ (crosses) for two uranium targets, in units of photons per bin per 1000 electrons, for a 2% X_0 (a) and 5% X_0 (b) thick target. The dotted line (top) shows the Bethe-Heitler Monte-Carlo expectation, whereas the dashed line (bottom) is the Monte-Carlo expectations including the LPM effect.

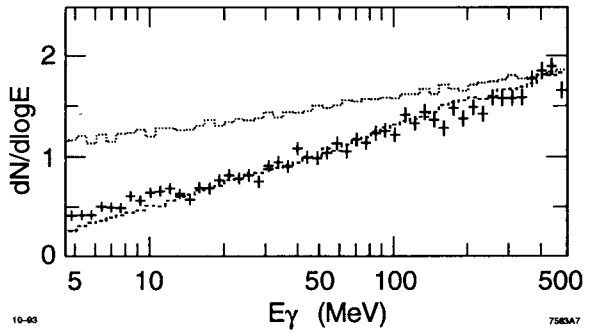

Figure 8: The difference between the bremsstrahlung spectra for the two uranium targets, with observed and expected spectra. Obtained by subtracting Figure 7(a) from Figure 7(b).

One can remove these surface effects from the data by subtracting the spectra for two targets of different thicknesses, at the price of a larger statistical error. In principle, the subtraction should leave 68 μm $\simeq 2\%X_0$ of bulk uranium in the middle of the target, without any surface effects. Figure 8 shows the difference between the spectra for $5\%X_0$ and $3\%X_0$ uranium targets. The data follows the LPM effect prediction very closely, and only diverges slightly below 10 MeV. The likely reason

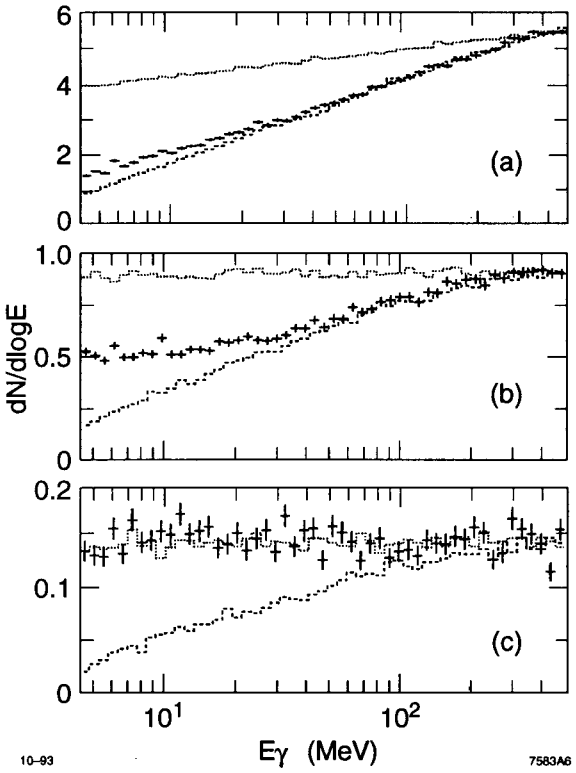

Figure 9: The observed bremsstrahlung spectrum $dN/d\log E$ (crosses) for three gold targets, in units of photons per bin per 1000 electrons, for 6% X_0 (a), 1% X_0 (b) and 0.1% X_0 (c) thick targets. The dotted line (top) shows the Bethe-Heitler Monte-Carlo expectation, whereas the dashed line (bottom) is the Monte-Carlo expectation including the LPM effect for bulk material.

for this disagreement is that the multi-photon pileup in the expected spectrum is calculated without taking the surface effects into account.

4.2. Thin Targets

To study how the LPM effect disappears for thin targets, we measured the bremsstrahlung spectrum for three gold targets; gold was chosen because it is dense and readily available in very thin foils. The results are shown in Fig. 9: part (a) for $203\,\mu\text{m} \simeq 6\%X_0$, part (b) for $25\,\mu\text{m} \simeq 1\%X_0$, and part (c) for $4\,\mu\text{m} \simeq 0.1\%X_0$ thick foils. The $6\%X_0$ target shows behaviour similar to the uranium targets: the data follow the curve expected for the LPM effect nicely, but exceed it slightly below $\approx$20 MeV. The $1\%X_0$ target shows much more of an excess below $\approx$50 MeV and seems to flatten out as would be expected for a Bethe-Heitler spectrum. The bulk of the data for the thinnest of the gold targets, $0.1\%X_0$ has not been analyzed yet; only a small data set is used here. The spectrum is clearly compatible with the Bethe-Heitler spectrum and not with LPM suppression. Unfortunately, our theoretical knowledge does not enable us to calculate the expected spectrum in the intermediate case in which the formation zone length is comparable to the target thickness. It is clear from

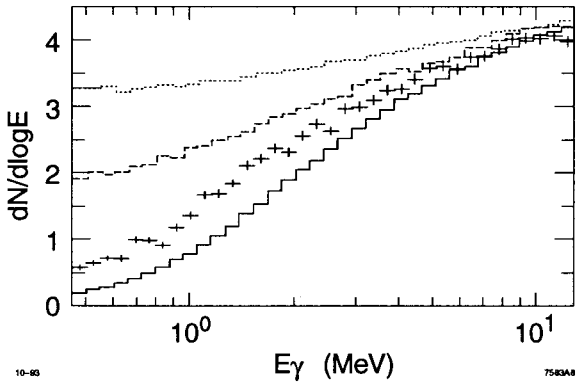

Figure 10: Bremsstrahlung spectrum from a 6% X_0 carbon target, for the energy range 0.5–10 MeV. Three Monte-Carlo expectation lines are shown, dotted at the top for Bethe-Heitler, dot-dashed in the middle for LPM suppression only, and solid at the bottom for LPM and dielectric suppression.

these figures that quantum-mechanical suppression effects vanish for thin targets, restoring the flat Bethe-Heitler spectrum.

4.3. Dielectric Suppression

For this study, the gain of the calorimeter was increased by a factor of about 10, so the usable range of energies is 0.5–50 MeV. This data contains significant contamination from synchrotron radiation. In order to suppress it, we exploit the fact that the spectrometer magnet creates a synchrotron radiation fan which starts at the center of the calorimeter and extends down; this is clearly visible in the observed angular distribution of bremsstrahlung photons. To suppress the synchrotron radiation, all energy clusters with centers in the bottom half of the calorimeter are discarded. Since the dielectric effect depends much less on density and X_0 than the LPM effect, it is most easily observed in light target materials, where LPM suppression is minimized. Preliminary results from this analysis on the $6\%X_0$ carbon target at 25 GeV beam energy are shown in Fig. 10. There are three Monte-Carlo spectra in this figure: Bethe-Heitler (dotted) at the very top, LPM suppression only (dot-dashed) in the center, and both LPM and dielectric suppression (dashed) at the very bottom. The Bethe-Heitler spectrum is clearly ruled out. Also ruled out is the observed data consisting of the LPM effect spectrum plus a background contribution. The figure is very suggestive of dielectric suppression with a significant background contamination. A more detailed analysis of dielectric suppression, using the 8 GeV data, is in progress.

5. Conclusions

We have performed an experiment to study the bremsstrahlung of low-energy photons from 25 GeV electrons, in which quantum-mechanical suppression is predicted. The analysis is still in progress, and all results presented here are preliminary. A final precision of a few percent in both energy scale and absolute cross-section measurement is expected.

The data shows quantitative agreement between the observed photon spectrum and the theory of LPM suppression for photon energies between 20 and 500 MeV. Below 20 MeV, surface effects modify the spectrum for heavy target materials, as is to be expected. In very thin targets, LPM suppression disappears, and the Bethe-Heitler spectrum is restored. The data is strongly suggestive of dielectric suppression occurring at about the predicted level.

In the process, we developed a method to generate a low-intensity high-energy parasitic electron beam while the SLAC accelerator operates in SLC/SLD mode. This beam is stable, controllable, and can be used for many purposes.

6. Acknowledgements

As can be seen from the author list, this is a very small collaboration. This experiment would have never been possible without the help of many people, among them Tony Bell, Don Briggs, Jerry Davis, Frank Dietrich, Roger Erickson, Roger Gearhart, Carl Hudspeth, Walter Kapica, Walter Meyerhof, Tom Nakashima, Gerard Putallaz, Mark Petree, Ben Smith, Dave Spooner, Mike Stanek, Ron Stickley, Steve St. Laurent, and Jack Truher. Our special appreciation goes to the MCC operations crew and the power conversion department, who established, operated, and maintained the beam line.

7. References

[1] See W. Heitler, *The Quantum Theory of Radiation* (Oxford University Press, 1936).
Reprinted: 3rd edition (Dover Publications, New York, 1984).

[2] E.L. Feinberg and I. Pomeranchuk, *Nuovo Cimento Suppl.* **3** (1956) 652.

[3] L.D. Landau and I.J. Pomeranchuk, *Dokl. Akad. Nauk. SSSR* **92**, (1953) 535, and *Dokl. Akad. Nauk. SSSR* **92**, 735 (1953).
These two papers are translated into English in *The collected Papers of L.D. Landau* (Pergamon Press, 1965).

[4] A.B. Migdal, *Phys. Rev.* **103** (1956), 1811.

[5] M.L. Ter-Mikaelian, *Dokl. Akad. Nauk. SSSR* **94** (1954) 1033.
For a discussion in English, see M.L. Ter-Mikaelian, *High Energy Electromagnetic Processes in Condensed Media* (John Wiley & Sons, 1972).

[6] F.F. Ternovskii, *Sov. Phys. JETP* **12** (1960) 123.

[7] T. Stanev *et al.*, *Phys. Rev.* **D25** (1982) 1291.

[8] W.R. Nelson, H.-Yirayama, and D.W.O. Rogers, SLAC–Report 265 (1985).

[9] P.H. Fowler *et al., Phil. Mag.* **4**, 1030 (1959);
S.C. Strausz *et al., Proc. 22nd ICRC* (Dublin, August 1991).

[10] A. Varfolomeev *et al., Sov. Phys. JETP* **42** (1976), 218.

[11] F.R. Arutyunyan, A.A. Nazarayan, and A.A. Frangyan, *Sov. Phys. JETP* **35** (1972) 1067.

[12] P. Chen and S.R. Klein, *Proc. 3rd Intl. Workshop on Advanced Accelerator Concepts* (Port Jefferson, New York, June 1992).

[13] S. Brodsky and P. Hoyer, *Phys. Lett.* **B298** (1993) 165.

[14] See *Proc. Workshop on High-Energy Neutrino Astronomy*, Honolulu, March 23–26, 1992 (World Scientific, Singapore, 1992).

[15] A. Misaki, *Fortschr. Phys.* **38** (1990) 413, and references therein.

[16] E. Konishi *et al., J. Phys. G* **17** (1991) 719, and references therein.

[17] Generously provided by Prof. Walter Meyerhof of Stanford University.

[18] I. Kirkbride, *SLAC Users Bulletin* **97** (1984) 10–11.

[19] First suggested by Al Odian, *personal communication.*

[20] S.R. Klein *et al.*, SLAC–PUB–6387 (1993), submitted to the *IEEE Transactions on Nuclear Science.*